Rearrangements in Model Peptide-Type Radicals *via* Intramolecular Hydrogen-Atom Transfer

by **Damian Moran***[a][b], **Rebecca Jacob**[c], **Geoffrey P. F. Wood**[a][b], **Michelle L. Coote**[b][c], **Michael J. Davies**[b][d], **Richard A. J. O'Hair**[b][e], **Christopher J. Easton**[b][c], and **Leo Radom***[a][b][c]

[a]) School of Chemistry, University of Sydney, Sydney, NSW 2006, Australia (e-mail: dmoran@chem.usyd.edu.au; radom@chem.usyd.edu.au)
[b]) ARC Centre of Excellence in Free Radical Chemistry and Biotechnology
[c]) Research School of Chemistry, Australian National University, Canberra, ACT 0200, Australia
[d]) Heart Research Institute, Camperdown, NSW 2050, Australia
[e]) School of Chemistry, Bio21 Institute, University of Melbourne, Victoria 3010, Australia

In fond memory of our friend and colleague, Professor *Hanns Fischer*, and in recognition of his distinguished contributions to chemistry

Intramolecular H-atom transfer in model peptide-type radicals was investigated with high-level quantum-chemistry calculations. Examination of 1,2-, 1,3-, 1,5-, and 1,6[C ↔ N]-H shifts, 1,4- and 1,7[C ↔ C]-H shifts, and 1,4[N ↔ N]-H shifts (*Scheme 1*), was carried out with a number of theoretical methods. In the first place, the performance of UB3-LYP (with the 6-31G(*d*), 6-31G(*2df,p*), and 6-311+G(*d,p*) basis sets) and UMP2 (with the 6-31G(*d*) basis set) was assessed for the determination of radical geometries. We found that there is only a small basis-set dependence for the UB3-LYP structures, and geometries optimized with UB3-LYP/6-31G(*d*) are generally sufficient for use in conjunction with high-level composite methods in the determination of improved H-transfer thermochemistry. Methods assessed in this regard include the high-level composite methods, G3(MP2)-RAD, CBS-QB3, and G3//B3-LYP, as well as the density-functional methods B3-LYP, MPWB1K, and BMK in association with the 6-31+G(*d,p*) and 6-311++G(*3df,3pd*) basis sets. The high-level methods give results that are close to one another, while the recently developed functionals MPWB1K and BMK provide cost-effective alternatives. For the systems considered, the transformation of an N-centered radical to a C-centered radical is always exothermic (by 25 kJ·mol^{-1} or more), and this can lead to quite modest barrier heights of less than 60 kJ·mol^{-1} (specifically for 1,5[C ↔ N]-H and 1,6[C ↔ N]-H shifts). H-Migration barriers appear to decrease as the ring size in the transition structure (TS) increases, with a lowering of the barrier being found, for example when moving from a rearrangement proceeding *via* a four-membered-ring TS (*e.g.*, the 1,3[C ↔ N]-H shift, $CH_3-C(O)-NH^{\bullet} \rightarrow {}^{\bullet}CH_2-C(O)-NH_2$) to a rearrangement proceeding *via* a six-membered-ring TS (*e.g.,* the 1,5[C ↔ N]-H shift, ${}^{\bullet}NH-CH_2-C(O)-NH-CH_3 \rightarrow NH_2-CH_2-C(O)-NH-CH_2{}^{\bullet}$).

1. Introduction. – Radicals are ubiquitous in biological systems and have been shown to be involved in a wide range of important reactions [1]. For instance, the first committed step in DNA biosynthesis is catalyzed by the enzyme ribonucleotide reductase in a radical-based mechanism. Radical reactions are also involved in a variety of degenerative physiological disorders [2], including atherosclerosis [3], cataractogenesis [4], *Alzheimer*'s disease, and *Creutzfeldt–Jacob* disease [5][6].

There have been a number of previous experimental studies on peptide radical rearrangements. Among these is the work of *Davies* and co-workers [7][8], who used EPR spectroscopy to monitor experiments such as hypochlorite oxidation of amino acids and peptides to investigate their radical decomposition and rearrangement processes. They proposed that N-centered radicals (N-radicals) of lysine rearrange to C-centered radicals (C-radicals) *via* 1,5[C ↔ N]-H shifts and possibly 1,2[C ↔ N]-H shifts [8]. The formation of C(β)-centered radicals was confirmed under slightly basic conditions (pH 7.4) *via* a putative 1,5[C ↔ N]-H shift from a side-chain aminyl N-radical involving a six-membered-ring transition structure. On the other hand, C(α)-radical formation was confirmed at low pH (<6), possibly *via* a 1,2[C ↔ N]-H shift from a side chain or N-terminal aminyl N-radical [8]. Another notable contribution dealing with peptide radical rearrangements is the intramolecular H-transfer work of *Turecek* and co-workers [9]. They examined H-atom transfer from the ammonium N-terminus in β-alanine amide and *N*-methylacetamide radicals, and found that migration of an ammonium H-atom was competitive with its dissociation from gas-phase peptide radicals. In other related studies, *Cohen* and co-workers [10] and *Curran* and co-workers [11] reported that intramolecular H-transfer rates in some substrates are faster than the rates for isomerization *via* hindered internal rotation. For example, in substrates with an amide bond connecting the sites that participate in a 1,5[C ↔ N]-H shift, it was found that the H-migration rate was faster than amide C–N bond rotation, and this was reflected both in reaction isotope effects and product ratios [11].

As a prelude to a broader computational exploration of peptide radical rearrangements, we computed thermochemical parameters (*Fig. 1*) associated with intramolecular H-atom migrations **A**–**G** (see *Scheme 1*) in model systems that correspond to fragments **1**–**14** of a glycine dipeptide (*Scheme 1*, inset). These allow 1,2-, 1,3-, 1,5-, and 1,6[C ↔ N]-H shifts (see **1**–**8**), 1,4- and 1,7[C ↔ C]-H shifts (see **9**–**12**), and 1,4[N ↔ N]-H shifts (see **13** and **14**) to be examined. As part of this study, the performance of a variety of methods for determining the geometries of the species involved (*e.g.*, UB3-LYP, UMP2), as well as the H-rearrangement thermochemistry (*e.g.*, MPWB1K, BMK, G3(MP2)-RAD) was assessed.

We emphasize at the outset that the truncated model reactions **A**–**G** have only a modest chemical resemblance to the reactions within a peptide-backbone radical, as

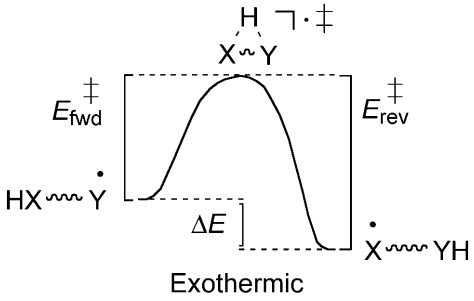

Fig. 1. *Graphical summary of labels used to describe reaction enthalpies* (ΔE) *and forward* ($E_{fwd}^{\ddagger}$) *and reverse* ($E_{rev}^{\ddagger}$) *barriers for [X ↔ Y]-H shifts in model peptide-type radicals, written in the exothermic direction*

Scheme 1. *Possible H-Atom Migrations* **A**–**G** *Associated with Model Fragments* **1**–**14**[a]) *of a Glycine Dipeptide Radical*

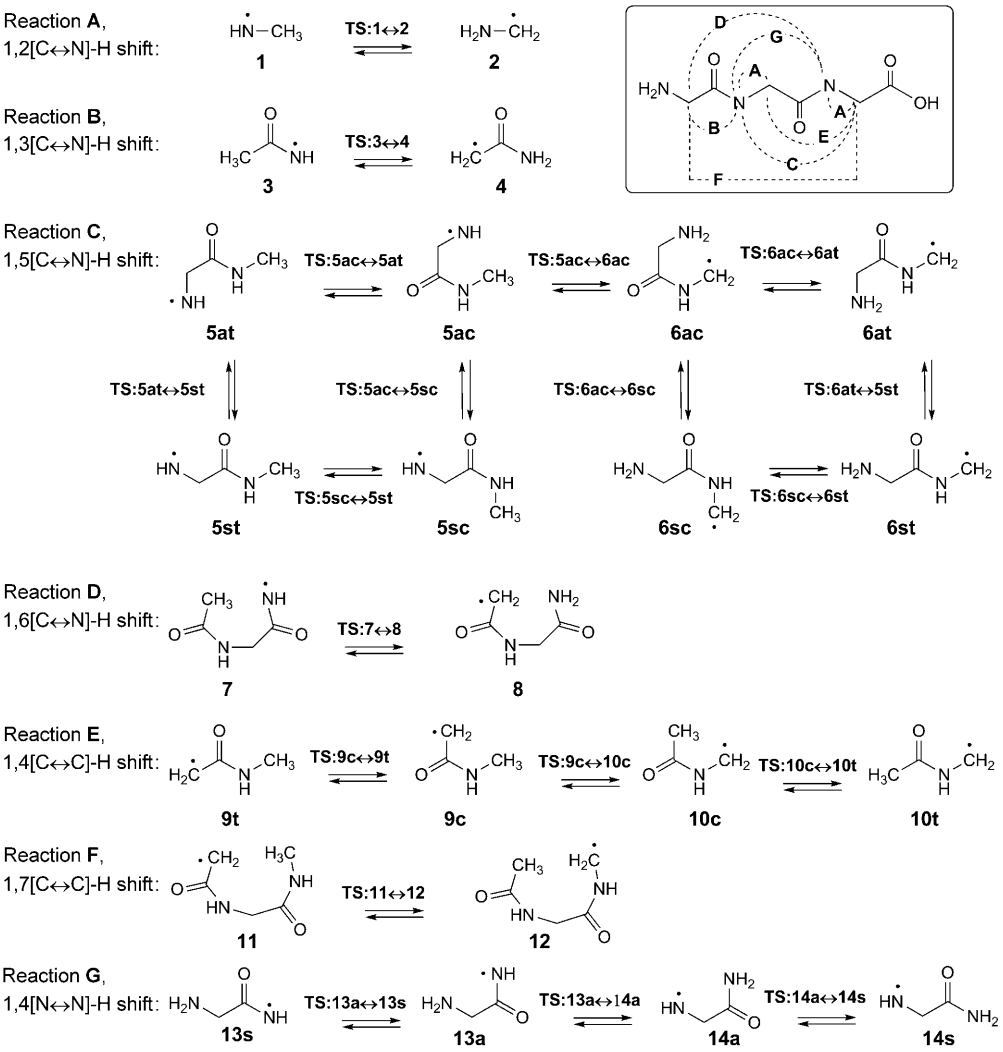

[a]) The following short-form labels are used: **s** = *syn*-periplanar, **a** = *anti*-periplanar, **c** = *cis*, **t** = *trans*, **sc** = *syn*-periplanar and *cis*, **st** = *syn*-periplanar and *trans*, **ac** = *anti*-periplanar and *cis*, **at** = *anti*-periplanar and *trans*. The terms *syn*-periplanar/*anti*-periplanar refer to the relationship of C=O to the vicinal N-terminus, and *cis*/*trans* refer to the relationship of the chain termini with respect to the amide C–N bond.

the N- and C-terminal radicals are capped in our systems with H-atoms. Reaction **G**, for example, which is used to model an intramolecular 1,4[N ↔ N]-H transfer, will obviously have a distinctly different thermochemical profile to a 1,4[N ↔ N]-H shift between two amide groups in the 'real' peptide. However, examination of these systems is a productive first step to modeling peptide-backbone-radical rearrangement proc-

esses. In particular, their computationally tractable size (*i.e.*, small number of electrons) and their relatively modest conformational complexity allows the use of high-level theoretical procedures, which in turn enables the assessment of computationally less demanding methods. Examination of systems that more closely model rearrangements within a peptide is in progress.

Our general strategy is to determine the transition structures (TSs) for H-atom transfer and then follow the reaction path downhill on both sides of the TS to determine which conformational minima it joins. In three cases (reactions **C**, **E**, and **G**), we do additional exploration to find out how much energy is involved in the preorganization required to move from an extended structure to such *cis*/*syn* periplanar type structures *via trans* → *cis* and *anti*-periplanar → *syn*-periplanar rearrangements. As found previously [10][11], barriers for such processes may represent a significant impediment to H-atom migrations in peptide radicals. We note that radical decomposition reactions were not considered within the present study.

2. Computation Details. – *Ab initio* molecular-orbital-theory [12] and density-functional-theory [13] calculations were carried out with the Gaussian03 [14] and MOLPRO 2002.6 [15] program packages. Radicals were typically treated with an unrestricted wave function, denoted 'U' (*e.g.*, UB3-LYP). When a restricted-open-shell wave function was employed, an 'R' prefix (*e.g.*, RB3-LYP) is used. Except where full calculations were required as part of a standard composite method, the frozen-core approximation was employed. Unless stated otherwise, we used UB3-LYP/6-31G(*d*) geometries and scaled (by 0.9806 [16]) zero-point-vibrational-energy (*ZPVE*) corrections.

The influence of geometry on reaction energies (ΔE) and rearrangement barriers ($E^{\ddagger}_{\mathrm{fwd}}$ and $E^{\ddagger}_{\mathrm{rev}}$) was assessed by computing high-level single-point energies on geometries optimized at a variety of lower levels. Specifically, equilibrium structures and transition structures (*Scheme 1*) were located at the UMP2/6-31G(*d*), UB3-LYP/6-31G(*d*), UB3-LYP/6-31G(*2df*,*p*), and UB3-LYP/6-311+G(*d*,*p*) levels of theory, followed by energy calculations on the optimized geometries with UB3-LYP/6-311++G(3*df*,2*p*) and the URCCSD(T)/6-311+G(*d*,*p*) procedure of MOLPRO (which involves unrestricted coupled cluster calculations on RHF wave functions) (*Tables 1* and *2*). The performance of both lower-cost methods (*e.g.*, BMK [17], MPWB1K [18], B3-LYP, and RMP2) and computationally more demanding methods (*e.g.*, G3//B3-LYP [19], G3(MP2)-RAD [20][21], and CBS-QB3 [22]) were then evaluated in relation to the prediction of radical relative energies and H-transfer barriers. Unless stated otherwise, energies within the text refer to G3(MP2)-RAD values at 0 K. We note that G3(MP2)-RAD was originally introduced [21] to give an improved description of radicals, and in particular eliminates the UMP2 aspects of standard G3(MP2).

3. Results and Discussion. – 3.1. *Theory Assessment.* 3.1.1. *Geometry Optimization Methodologies.* The influence of the method used for geometry optimization on computed thermochemical parameters was assessed by calculating single-point URCCSD(T)/6-311+G(*d*,*p*) and UB3-LYP/6-311++G(*3df*,*2p*) energies on geometries optimized with a variety of procedures. The resultant thermochemical parameters are presented in *Tables 1* and *2*.

Table 1. *Effect of Geometry on Calculated Thermochemical Parameters* (URCCSD(T)/6-311+G(*d*,*p*) and UB3-LYP/6-311++G(3*df*,2*p*); in kJ·mol^{-1}) *for [C ↔ N]-H Shifts*[a])

	Optimization level	URCCSD(T)/6-311+G(*d*,*p*)			UB3-LYP/6-311++G(3*df*,2*p*)		
		$E^{\ddagger}_{fwd}$	ΔE	$E^{\ddagger}_{rev}$	$E^{\ddagger}_{fwd}$	ΔE	$E^{\ddagger}_{rev}$
1,2[C ↔ N]-H Shift (**A**):	UB3-LYP/6-31+G(*d*,*p*)	171.1	−24.7	195.8	163.8	−31.1	194.9
	UB3-LYP/6-31G(2*df*,*p*)	171.0	−25.3	196.3	163.9	−30.6	194.5
	UB3-LYP/6-31G(*d*)	170.9	−25.2	196.1	163.8	−30.2	194.0
	UMP2/6-31G(*d*)	171.7	−25.1	196.8	164.1	−29.9	194.0
1,3[C ↔ N]-H Shift (**B**):	UB3-LYP/6-31+G(*d*,*p*)	166.9	−47.3	214.1	159.0	−55.6	214.7
	UB3-LYP/6-31G(2*df*,*p*)	166.5	−48.0	214.5	158.9	−55.7	214.6
	UB3-LYP/6-31G(*d*)	166.5	−48.3	214.8	158.6	−55.7	214.3
	UMP2/6-31G(*d*)	164.5	−49.5	214.0	154.5	−61.4	216.0
1,5[C ↔ N]-H Shift (**C**):	UB3-LYP/6-31+G(*d*,*p*)	74.0	−21.5	95.5	61.0	−30.7	91.7
	UB3-LYP/6-31G(2*df*,*p*)	73.7	−22.9	96.6	60.9	−30.2	91.0
	UB3-LYP/6-31G(*d*)	73.4	−23.0	96.4	60.6	−30.2	90.8
	UMP2/6-31G(*d*)	74.5	−22.4	97.0	61.4	−29.6	91.0
1,6[C ↔ N]-H Shift (**D**):	UB3-LYP/6-31+G(*d*,*p*)	59.5	−59.5	119.0	48.0	−64.1	112.2
	UB3-LYP/6-31G(2*df*,*p*)	57.9	−61.1	119.0	48.2	−64.1	112.1
	UB3-LYP/6-31G(*d*)	58.7	−60.9	119.5	47.5	−64.2	111.7
	UMP2/6-31G(*d*)	56.6	−62.3	118.9	39.0	−72.4	111.4

[a]) Relative energies do not include *ZPVE* corrections.

Table 2. *Effect of Geometry on Calculated Thermochemical Parameters* (URCCSD(T)/6-311+G(d,p) and UB3-LYP/6-311++G(3df,2p), kJ·mol^{-1}) *for [C ↔ C]-H and [N ↔ N]-H Shifts*[a])

	Optimization level	URCCSD(T)/6-311+G(*d*,*p*)			UB3-LYP/6-311++G(3*df*,2*p*)		
		$E^{\ddagger}_{fwd}$	ΔE	$E^{\ddagger}_{rev}$	$E^{\ddagger}_{fwd}$	ΔE	$E^{\ddagger}_{rev}$
1,4[C ↔ C]-H Shift (**E**):	UB3-LYP/6-31+G(*d*,*p*)	110.4	−23.5	133.9	106.9	−28.3	135.1
	UB3-LYP/6-31G(2*df*,*p*)	110.5	−23.6	134.1	106.9	−28.2	135.1
	UB3-LYP/6-31G(*d*)	110.6	−23.8	134.3	106.9	−28.0	134.9
	UMP2/6-31G(*d*)	110.5	−25.1	135.6	106.8	−27.0	133.8
1,7[C ↔ C]-H Shift (**F**):	UB3-LYP/6-31+G(*d*,*p*)	79.2	−19.4	98.6	81.2	−24.4	105.7
	UB3-LYP/6-31G(2*df*,*p*)	78.4	−19.6	98.0	81.3	−24.4	105.6
	UB3-LYP/6-31G(*d*)	78.7	−19.4	98.1	81.3	−24.3	105.6
	UMP2/6-31G(*d*)	78.4	−20.3	98.7	81.3	−23.5	104.8
1,4[N ↔ N]-H Shift (**G**):	UB3-LYP/6-31+G(*d*,*p*)	50.9	−60.9	111.8	35.4	−55.2	90.6
	UB3-LYP/6-31G(2*df*,*p*)	52.4	−59.4	111.8	35.6	−54.9	90.6
	UB3-LYP/6-31G(*d*)	51.0	−60.6	111.5	35.3	−55.4	90.7
	UMP2/6-31G(*d*)	54.5	−60.6	115.1	41.1	−68.2	109.4

[a]) Relative energies do not include *ZPVE* corrections.

We can see that the URCCSD(T)/6-311+G(*d*,*p*)//UB3-LYP energies show minimal (<5 kJ·mol^{-1}) variation with respect to the level of optimization. This is also the case for the UB3-LYP/6-311++G(*3df*,*2p*)//UB3-LYP energies, with energy ranges of less

than 2 kJ·mol^{-1}. However, when the single-point energies obtained with UB3-LYP- and UMP2-optimized geometries are compared, there are significant differences in reaction enthalpies and barrier heights in some cases. For example, for the 1,3[C ↔ N]-H shift, there are differences of *ca.* 6 kJ·mol^{-1} in ΔE and *ca.* 4 kJ·mol^{-1} in $E^{\ddagger}_{fwd}$, while for the 1,6[C ↔ N]-H shift, the differences are *ca.* 8 kJ·mol^{-1} (ΔE) and *ca.* 9 kJ·mol^{-1} ($E^{\ddagger}_{fwd}$). The most dramatic disparity between energies obtained by using the UB3-LYP- and UMP2-optimized geometries occurs for the 1,4[N ↔ N]-H shift, with a difference of *ca.* 19 kJ·mol^{-1} between the respective UB-3LYP/6-311++G(*3df,2p*) values for $E^{\ddagger}_{rev}$.

To probe this apparent discrepancy further, **TS:13a** ↔ **14a** was also optimized with UQCISD/6-31G(*d*), followed by URCCSD(T)/6-311+G(*d,p*) and UB-3LYP/6-311++G(*3df,2p*) energy evaluations (*Fig. 2*). For **14a**, both the URCCSD(T)/6-311+G(*d,p*) and UB3-LYP/6-311++G(*3df,2p*) total energies show relatively little dependence on the level of geometry optimization, lying within a 1 kJ·mol^{-1} range in each case. This is consistent with the small variation in geometries for **14a** seen in *Fig. 2*. For **13a**, both the UB3-LYP and UMP2 geometries lead to high URCCSD(T) energies (*ca.* 7 kJ·mol^{-1} above that given for the UQCISD geometry), while the UMP2 geometry gives a high UB3-LYP energy (*ca.* 10 kJ·mol^{-1} above that given by the UQCISD geometry). For **TS:13a** ↔ **14a**, the UMP2 geometry leads to a very high UB3-LYP energy (*ca.* 18 kJ·mol^{-1} above that given by the UQCISD geometry). Consistent with these results, greater variation can be seen in the optimized structures for **13a** and **TS:13a** ↔ **14a** than for **14a** (*Fig. 2*). We note in particular the significant variations in the C–C(O)–N–H dihedral angles in **13a** and the N···H···N bond lengths in **TS:13a** ↔ **14a**.

Overall, the QCISD geometries always lead to the lowest URCCSD(T) energy and close to the lowest UB3-LYP energy. The UB3-LYP geometries are not quite as reliable but appear to lead to only modest errors in energies. UMP2 geometries can sometimes lead to significant energy errors.

If the results obtained by using UB3-LYP geometries with various basis sets are compared, the general observation is that the variation in calculated thermochemical parameters is small. Examination in more detail of the calculated total energies shows that the UB3-LYP/6-311+G(*d,p*) geometry optimizations produce structures with lower UB3-LYP/6-311++G(*3df,2p*) energies than the UB3-LYP/6-31G(*d*) and UB3-LYP/6-31G(*2df,p*) structures. In contrast, at the URCCSD(T)/6-311+G(*d,p*) level, the UB3-LYP geometry that gives the lowest absolute energies is typically UB3-LYP/6-31G(*d*).

3.1.2. *Thermochemical Parameters.* To compare the performance of the high-level methods in predicting the thermochemical parameters, we use G3(MP2)-RAD as our reference procedure. The mean absolute deviations (*MAD*s), mean deviations (*MD*s), and largest deviations (*LD*s) of G3//B3-LYP and CBS-QB3 values from enthalpies and barriers calculated with G3(MP2)-RAD for reactions **A**–**G** are summarized in *Table 3*. Note that the sign convention that we use is deviation(method) = value(method) – value(G3(MP2)-RAD). As expected, the *MAD*s calculated with high-level methods are small (up to 3.3 kJ·mol^{-1}), indicating that the results obtained with the high-level methods are generally close to one another. The *LD* values indicate that there are occasional cases with larger deviations.

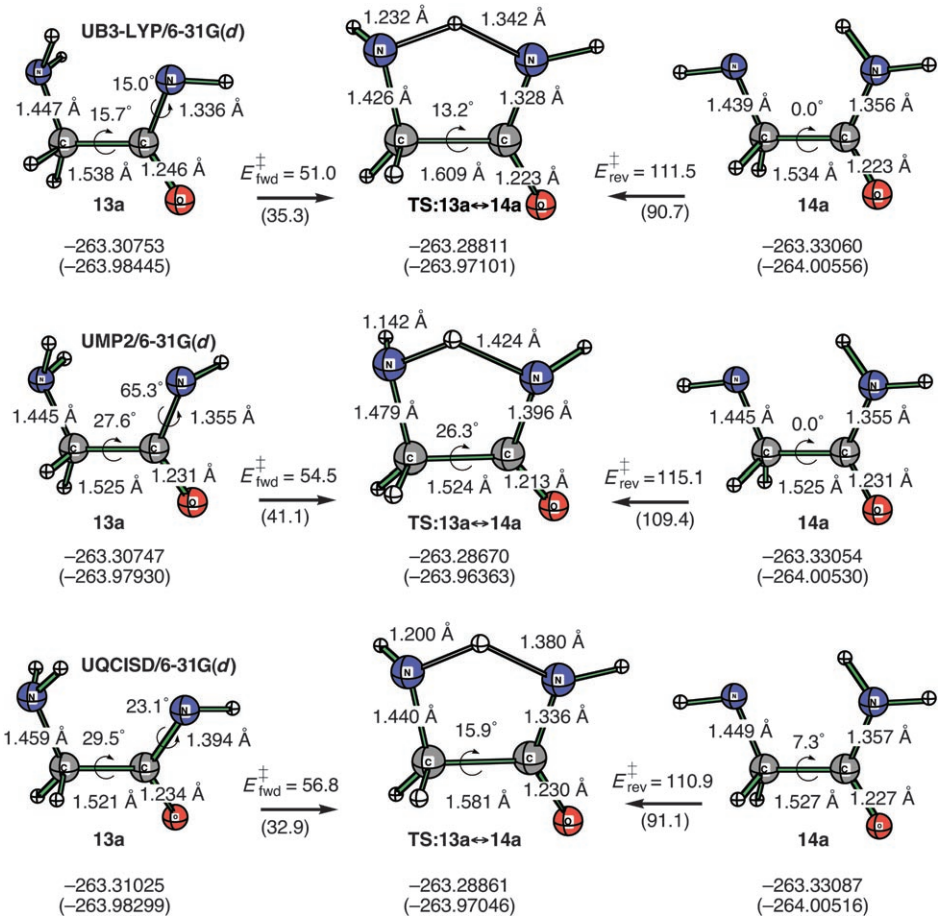

Fig. 2. *UB3-LYP/6-31G*(d)*, UMP2/6-31G*(d) *and UQCISD/6-31G*(d) *Optimized geometries of isomers* **13a** *and* **14a** *involved in the 1,4[N ↔ N]-H shift and their connecting transition structure* **TS:13a ↔ 14a**. Also shown are the URCCSD(T)/6-311+G(*d*,*p*) and (in parentheses) UB3-LYP/6-311++G(3*df*, 2*p*) total energies [Hartrees] and rearrangement barriers [kJ·mol^{-1}]. Relative energies do not include *ZPVE* corrections.

Turning now to the performance of the density functionals relative to G3(MP2)-RAD (*Table 4*), we see that UBMK and UMPWB1K do a particularly good job of reproducing the corresponding high-level thermochemical values. They show *MAD*s for the reaction enthalpies that are comparable to those for CBS-QB3 for these systems. Similarly, the agreement between UBMK/6-31+G(*d*,*p*) and UMPWB1K/6-31+G(*d*,*p*) barriers with G3(MP2)-RAD barriers is also very good. The energies predicted by UB3-LYP are not as good, with particularly large *LD*s (*Table 3*). Note that with one exception, the *MD*s for the BMK and MPWB1K enthalpies and barrier heights have opposite signs to the corresponding UB3-LYP values. This shows that UB3-LYP typically underestimates the barrier heights, while UBMK and UMPWB1K tend to overestimate them.

Table 3. *Comparison of the Performance of G3//B3-LYP, CBS-QB3, and B3-LYP Relative to G3(MP2)-RAD in the Prediction of H-Transfer Thermochemical Parameters* (0 K; in kJ·mol^{-1})[a])[b])

		G3//B3-LYP	CBS-QB3	UB3-LYP /lge[c])	RB3-LYP /lge[c])	UB3-LYP /sml[d])
$E^{\ddagger}_{fwd}$	*MAD*	2.4	2.7	4.2	4.6	5.8
	MD	0.0	−0.7	−3.7	−3.9	−3.1
	LD	−7.0	+5.1	−8.1	−9.9	−9.5
		1,3[C ↔ N]	1,4[N ↔ N]	1,5[C ↔ N]	1,4[N ↔ N]	1,5[C ↔ N]
ΔE	*MAD*	0.8	1.9	4.5	4.0	4.6
	MD	0.0	+0.5	+2.4	+0.5	+4.6
	LD	−1.3	+4.0	+14.9	+12.2	+15.6
		1,2[C ↔ N]	1,4[N ↔ N]	1,4[N ↔ N]	1,4[N ↔ N]	1,4[N ↔ N]
$E^{\ddagger}_{rev}$	*MAD*	2.6	3.3	6.9	7.0	8.7
	MD	+2.1	−1.1	−6.0	−4.3	−7.6
	LD	+5.9	−6.7	−22.5	−22.0	−23.0
		1,3[C ↔ N]	1,4[N ↔ N]	1,4[N ↔ N]	1,4[N ↔ N]	1,4[N ↔ N]

[a]) Mean absolute deviations (*MAD*s), mean deviations (*MD*s), and largest deviations (*LD*s) are listed, as well as the rearrangement that contributes the largest deviation. [b]) UB3-LYP/6-31G(*d*) geometry and *ZPVE*. [c]) The 'lge' basis set is 6-311++G(*3df,3pd*). [d]) The 'sml' basis set is 6-31+G(*d,p*).

Table 4. *Comparison of the Performance of MPWB1K and BMK Relative to G3(MP2)-RAD in the Prediction of H-Transfer Thermochemical Parameters* (0 K; in kJ·mol^{-1})[a])[b])

		UBMK /lge[c])	RBMK /lge[c])	UBMK /sml[d])	UMPW-B1K /lge[c])	RMPW-B1K /lge[c])	UMPW-B1K /sml[d])
$E^{\ddagger}_{fwd}$	*MAD*	1.4	3.5	3.6	2.1	3.4	3.7
	MD	+0.4	0.0	−0.4	+0.8	+0.9	+2.7
	LD	+4.7	+7.0	+7.2	−3.9	−5.8	+7.6
		1,2[C ↔ N]	1,4[N ↔ N]	1,2[C ↔ N]	1,4[C ↔ C]	1,4[N ↔ N]	1,3[C ↔ N]
ΔE	*MAD*	2.1	4.6	1.5	1.9	5.4	0.9
	MD	−2.1	−4.6	−1.2	−1.7	−5.4	−0.3
	LD	−5.5	−7.9	−4.2	−3.7	−12.2	−1.7
		1,7[C ↔ C]	1,4[N ↔ N]	1,4[C ↔ C]	1,4[C ↔ C]	1,4[N ↔ N]	1,4[N ↔ N]
$E^{\ddagger}_{rev}$	*MAD*	3.0	4.7	2.9	3.0	6.3	4.0
	MD	+2.5	+4.7	+0.9	+2.5	+6.3	+3.1
	LD	+6.2	+8.6	+7.8	+6.7	+9.6	+7.8
		1,2[C ↔ N]	1,2[C ↔ N]	1,2[C ↔ N]	1,7[C ↔ C]	1,7[C ↔ C]	1,2[C ↔ N]

[a]) Mean absolute deviations (*MAD*s), mean deviations (*MD*s), and largest deviations (*LD*s) are listed, as well as the rearrangement that contributes the largest deviation. [b]) UB3-LYP/6-31G(*d*) geometry and *ZPVE*. [c]) The 'lge' basis set is 6-311++G(*3df,3pd*). [d]) The 'sml' basis set is 6-31+G(*d,p*).

Zhao and *Truhlar* [18] have recommended using MPWB1K in combination with the (small) 6-31+G(*d,p*) basis set, and the UMPWB1K/6-31+G(*d,p*) enthalpies are indeed slightly superior to the UMPWB1K/6-311++G(*3df,3pd*) values. However, the large-basis-set UMPWB1K barrier heights are in better agreement with G3(MP2)-RAD.

Boese and *Martin*'s BMK functional [17] also has superior *MAD*, *MD*, and *LD* values for enthalpies when combined with 6-31+G(*d*,*p*). In contrast to BMK and MPWB1K, UB3-LYP appears always to benefit from a large basis set for the systems examined, although the improvement is modest (<2 kJ·mol^{-1}).

It has previously been found that the restricted-open-shell RB3-LYP method gives enthalpies for reactions involving N-centered radicals that are in better agreement with results of high-level composite methods such as *Martin* and *Parthiban*'s W1 procedure [23] than are found with UB3-LYP [24]. We find here that RB3-LYP/6-311++G(*3df*,*3pd*) does indeed perform slightly better than UB3-LYP/6-311++G(*3df*,*3pd*) for reaction enthalpies, but it performs slightly worse for barriers. However, when the restricted-open-shell formalism is applied to either BMK or MPWB1K (*i.e.*, RBMK, RMPWB1K), the predicted enthalpies typically have significantly larger *MAD*s than those of their unrestricted counterparts.

3.2. *Hydrogen-Transfer Thermochemistry.* The thermochemical parameters for intramolecular H-atom transfer in the model reactions **A**–**G** are summarized in *Tables 5* and *6*. As a consequence of our assessment of methods (*vide supra*), discussion is limited to results with our high-level reference method G3(MP2)-RAD.

3.2.1. *General Considerations.* The stabilities of the peptide-type radicals depend on whether they are N-centered or C-centered, and on the substituents involved. In general, N-radicals are less stable than C-radicals (relative to corresponding closed-shell counterparts), which is reflected in the energy change for the reaction $NH_3 + {}^{\bullet}CH_3 \rightarrow {}^{\bullet}NH_2 + CH_4$ of 10.9 kJ·mol^{-1} (G3(MP2)-RAD, 0 K) or 12.7 kJ·mol^{-1} (experimental, 0 K, calculated from 298-K heats of formation listed in [25], back-corrected by using a scaled (by 0.9989 [16]) B3-LYP/6-31G(*d*) enthalpy temperature correction (of -0.7 kJ·mol^{-1})). Likewise, the N$^{\bullet} \rightarrow$ C$^{\bullet}$ 1,2-rearrangement (reaction **A**, *Scheme 1*) is exothermic ($\Delta E = -25.0$ kJ·mol^{-1}), and there is again good agreement with the experimental ΔE for reaction **A** of -23.6 kJ·mol^{-1} (calculated from experimental 298-K heats of formation given in [26], back-corrected by using a scaled B3-LYP/6-31G(*d*) enthalpy temperature correction (of -0.2 kJ·mol^{-1})).

As far as substituents are concerned, we have recently shown, using radical-stabilization energies (*RSE*s) as a measure of relative radical stability, that monosubstituted C-radicals are stabilized by both amino (44.5–49.5 kJ·mol^{-1}) and carbonyl (24.7–36.9 kJ·mol^{-1}) groups, with the amino substituents being the more effective stabilizing groups [27]. In combination, amino and carbonyl substituents on a disubstituted C-radical produce a large stabilizing effect, including a captodative (synergistic) interaction [5][28] of 12.8–39.4 kJ·mol^{-1} [27]. For monosubstituted N-radicals, on the other hand, we found that methyl and related (CH_2Z) groups have a stabilizing effect of 25.9–31.7 kJ·mol^{-1}, while electron-withdrawing carbonyl substituents are *de*stabilizing by 22.3–30.8 kJ·mol^{-1} [27]. An effective additional destabilization occurs for the disubstituted N-radicals of 7.8–18.6 kJ·mol^{-1}, leading to overall *RSE*s of -0.2 to -19.0 kJ·mol^{-1} [27].

To determine the preferred geometric arrangements for the transition structures for [C ↔ C]-H-, [C ↔ N]-H-, and [N ↔ N]-H-transfer reactions in the absence of other influences, we have examined the angular dependence of the barriers for the prototypical reactions, $CH_4 + {}^{\bullet}CH_3 \rightarrow {}^{\bullet}CH_3 + CH_4$, $CH_4 + {}^{\bullet}NH_2 \rightarrow {}^{\bullet}CH_3 + NH_3$, and $NH_3 + {}^{\bullet}NH_2 \rightarrow {}^{\bullet}NH_2 + NH_3$ [29]. The saddle points corresponding to H-transfer were determined

for a series of fixed values of the X···H···X angle, with all other geometric parameters being optimized (UB3-LYP/6-31G(*d*)), followed by single-point G3(MP2)-RAD energy calculations. The calculated geometries are displayed in *Fig. 3*, while the variations in energy as a function of the X···H···X bending angle are shown in *Fig. 4*. We can see that the TS geometries for H-transfer prefer linear ([C ↔ C]), or near-linear ([C ↔ N] and [N ↔ N]) arrangements (*Fig. 3*). In addition, it is clear that, whereas the potential curve for bending is relatively flat in the 160° to 180° region, the energy cost of distortion to smaller angles increases quite rapidly (*Fig. 4*). These observations suggest that there will be a significant energy penalty in the case of the H-transfer TSs for our peptide-type models when small rings are involved.

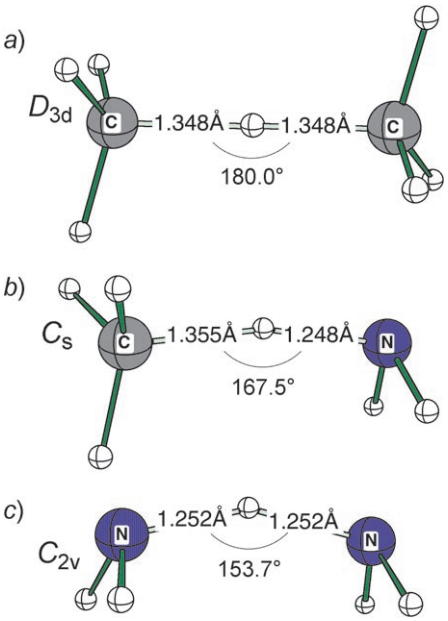

Fig. 3. *Optimized geometries* (UB3-LYP/6-31G(*d*)) *of H-transfer transition structures for prototypical reactions:* a) $CH_4 + {}^{\cdot}CH_3 \rightarrow {}^{\cdot}CH_3 + CH_4$, b) $CH_4 + {}^{\cdot}NH_2 \rightarrow {}^{\cdot}CH_3 + NH_3$, *and* c) $NH_3 + {}^{\cdot}NH_2 \rightarrow {}^{\cdot}NH_2 + NH_3$

3.2.2. *[C ↔ N] Shifts of H-Atoms.* The 1,2[C ↔ N]-H shift is exothermic ($\Delta E = -25.0\ kJ \cdot mol^{-1}$) and has a three-membered-ring transition structure (**TS:1** ↔ **2**) with a narrow N−H−C angle of 70.0° (*Fig. 5*). Not surprisingly in the light of the discussion above, the predicted forward ($E^{\ddagger}_{fwd} = 152.7\ kJ \cdot mol^{-1}$) and reverse ($E^{\ddagger}_{rev} = 177.6\ kJ \cdot mol^{-1}$) barriers for the 1,2[C ↔ N]-H shift are very high (*Table 5*). For comparison, barriers to an analogous *inter*molecular [C ↔ N]-H shift (*Scheme 2*) are 41.4 ($E^{\ddagger}_{fwd}$) and 66.4 $kJ \cdot mol^{-1}$ ($E^{\ddagger}_{rev}$), with an enthalpy change of $-25.0\ kJ \cdot mol^{-1}$. Our high calculated barrier for the 1,2[C ↔ N]-H shift suggests that the observed rearrangements of this type [8] are taking place by an alternative mechanism such as protonation/deprotonation.

As with the 1,2[C ↔ N]-H shift, 1,3-H migration between C- and N-radical centers (reaction **B**, *Scheme 1*) also favors formation of the C-radical. However, the N$^{\cdot}$ → C$^{\cdot}$ rearrangement is significantly more exothermic (in this case $\Delta E = -55.6\ kJ \cdot mol^{-1}$, see *Table 5*), reflecting the relative destabilization of the N-centered reactant radical

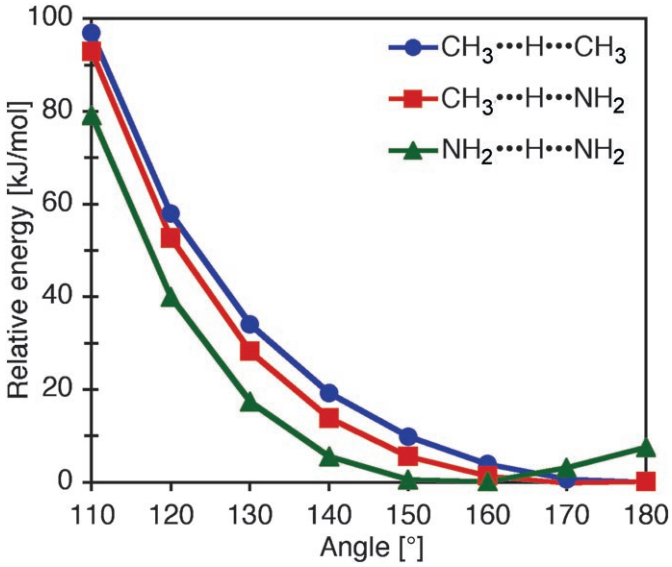

Fig. 4. *Dependence of barriers* (G3(MP2)-RAD, 0 K) *on X···H···X angle in the saddle points corresponding to H-transfer in the prototypical reactions:* a) $CH_4+{}^{\cdot}CH_3 \rightarrow {}^{\cdot}CH_3+CH_4$, b) $CH_4+{}^{\cdot}NH_2 \rightarrow {}^{\cdot}CH_3+NH_3$, *and* c) $NH_3+{}^{\cdot}NH_2 \rightarrow {}^{\cdot}NH_2+NH_3$ (see text)

Table 5. *Barriers* ($E^{\ddagger}_{fwd}$ *and* $E^{\ddagger}_{rev}$) *and Reaction Enthalpies* (ΔE) *for [C ↔ N]-H Shifts Computed at Various Levels of Theory* (0 K; in kJ·mol^{-1})[a])

	1,2[C ↔ N]-H Shift (**A**)			1,3[C ↔ N]-H Shift (**B**)			1,5[C ↔ N]-H Shift (**C**)			1,6[C ↔ N]-H Shift (**D**)		
	$E^{\ddagger}_{fwd}$	ΔE	$E^{\ddagger}_{rev}$	$E^{\ddagger}_{fwd}$	ΔE	$E^{\ddagger}_{rev}$	$E^{\ddagger}_{fwd}$	ΔE	$E^{\ddagger}_{rev}$	$E^{\ddagger}_{fwd}$	ΔE	$E^{\ddagger}_{rev}$
G3(MP2)-RAD	152.7	−25.0	177.6	143.9	−55.6	199.5	57.3	−28.6	85.9	42.1	−70.3	112.3
CBS-QB3	153.3	−27.8	181.1	149.0	−54.5	203.5	51.8	−30.2	82.0	43.4	−67.7	111.1
G3//B3-LYP	147.2	−26.3	181.5	150.8	−54.6	205.4	58.5	−28.8	87.3	43.8	−71.0	114.7
UBMK/6-311++G(*3df,3pd*)[b])	157.4	−26.5	183.8	144.2	−56.8	200.9	58.0	−28.5	86.4	41.0	−70.4	111.4
RBMK/6-311++G(*3df,3pd*)[b])	158.9	−27.4	186.2	142.9	−60.5	203.4	60.3	−28.7	89.1	37.8	−75.5	113.3
UBMK/6-31+G(*d,p*)[b])	159.9	−26.0	185.9	147.8	−55.0	202.8	54.5	−28.8	83.4	39.5	−70.1	109.6
UMPWB1K/6-311++G(*3df,3pd*)[b])	155.1	−26.3	181.4	145.7	−57.2	202.9	56.6	−28.0	84.6	43.1	−71.4	114.5
RMPWB1K/6-311++G(*3df,3pd*)[b])	157.1	−27.3	185.0	145.0	−62.7	207.6	60.6	−28.5	89.1	39.8	−78.6	118.4
UMPWB1K/6-31+G(*d,p*)[b])	160.2	−25.2	185.4	151.4	−55.0	206.4	56.3	−27.4	83.7	44.7	−70.0	114.8
UB3-LYP/6-311++G(*3df,3pd*)[b])	154.0	−30.5	180.8	144.6	−53.9	198.5	49.2	−28.5	77.7	36.5	−63.1	99.6
RB3-LYP/6-311++G(*3df,3pd*)[b])	155.2	−31.6	183.1	143.2	−57.6	200.8	50.4	−29.4	79.8	33.9	−67.1	110.9
UB3-LYP/6-31+G(*d,p*)[b])	158.0	−23.7	181.6	148.1	−50.8	198.9	47.8	−27.0	74.8	36.7	−61.4	98.0

[a]) See *Scheme 1*. [b]) UB3-LYP/6-31G(*d*) geometry and scaled *ZPVE*.

by the acetyl group. The ring atoms of the four-membered-ring transition structure for the 1,3[C ↔ N]-H shift (**TS:3** ↔ **4**, *Fig. 5*) are approximately planar (out-of-plane distortion $<1°$), but there is significant deviation of the internal angles from their ideal 90° values due to the relative rigidity of the amide carbonyl group. In addition, the nar-

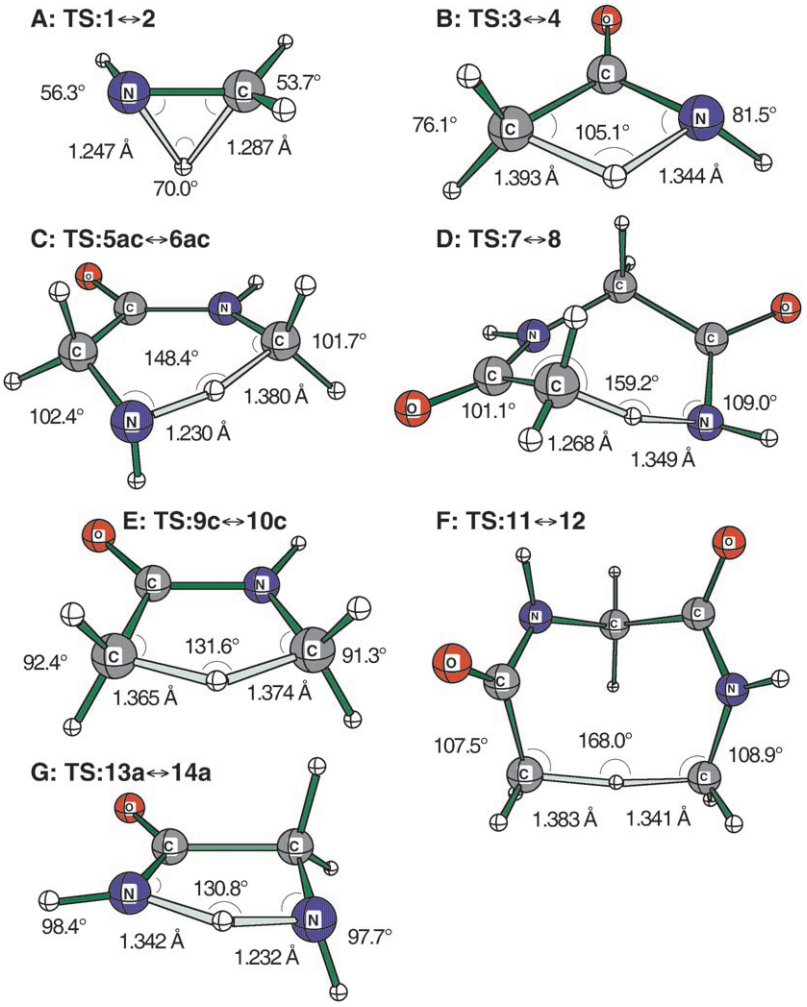

Fig. 5. *Optimized geometries* (B3-LYP/6-31G(*d*)) *of H-transfer transition structures*

row C–H–N angle of 105.1° contributes to the forward (143.9 kJ·mol^{-1}) and reverse (199.5 kJ·mol^{-1}) barriers again being very high.

The 1,5-rearrangement in reaction **C** is again exothermic ($\Delta E = -28.6$ kJ·mol^{-1}) as expected. Both the forward ($E^{\ddagger}_{fwd} = 57.3$ kJ·mol^{-1}) and reverse ($E^{\ddagger}_{rev} = 85.9$ kJ·mol^{-1}) 1,5[C ↔ N]-H shift barriers are relatively low compared with those for the 1,2[C ↔ N]-H and 1,3[C ↔ N]-H shifts (*Table 5*), which is likely to be associated with the comparatively low strain of the six-membered-ring TS of reaction **C** and a widened N–H–C angle of 148.4° (*Fig. 5*). The conformational preorganization required to get to **5ac** and from **6ac** is discussed in *Sect. 3.3*.

The 1,6[C ↔ N]-H shift of reaction **D** has a modest forward barrier ($E^{\ddagger}_{fwd} = 42.1$ kJ·mol^{-1}), a relatively large reaction exothermicity ($\Delta E = -70.3$ kJ·mol^{-1}) and a

Scheme 2. *Intermolecular [C ↔ N]-H Migration* via a) syn-*Periplanar and* b) anti-*Periplanar Transition Structures: G3(MP2)-RAD and* (in parenthesis) *CBS-QB3 Thermochemical Parameters* [kJ·mol^{-1}] *at 0 K*

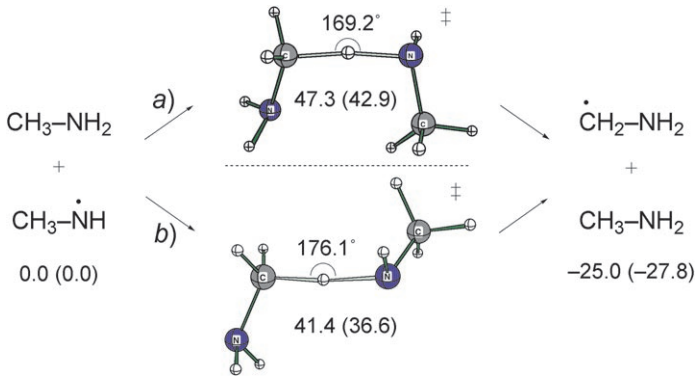

large reverse barrier ($E^{\ddagger}_{rev}$ = 112.3 kJ·mol^{-1}) (*Table 5*). The reactants and products of reaction **D** bear a strong resemblance to those for reaction **B**, and the ΔE value is similar. However, the geometry surrounding the transferred H-atom in the four-membered ring of **TS:3** ↔ **4** is more strained than that in the seven-membered-ring transition structure **TS:7** ↔ **8**, which also benefits from a widened C–H–N angle of 159.2° (*Fig. 5*). As a consequence, the $E^{\ddagger}_{fwd}$ and $E^{\ddagger}_{rev}$ values are *ca.* 80–100 kJ·mol^{-1} lower for reaction **D** than for reaction **B**.

3.2.3. *[C ↔ C] Shifts of H-Atoms.* Reaction **E** models a C(α) ↔ C(α) radical migration *via* a 1,4[C ↔ C]-H shift (*Scheme 1*). The rearrangement of **9c** to **10c** is moderately exothermic (ΔE = –25.7 kJ·mol^{-1}, see *Table 6*), reflecting the greater stabilization of C-radicals by adjacent N-atom lone-pair donors than by carbonyl acceptors [21][27][28]. The $E^{\ddagger}_{fwd}$ (98.6 kJ·mol^{-1}) and $E^{\ddagger}_{rev}$ (124.3 kJ·mol^{-1}) barriers to radical migration are large, perhaps associated with the quite narrow C–H–C angle of 131.6° (*Fig. 5*).

Reaction **F** also models a C(α) ↔ C(α) radical migration and is the largest system considered. It involves the 1,7[C ↔ C]-H shift between **11** and **12** *via* **TS:11** ↔ **12**. Structurally, **TS:9c** ↔ **10c** and **TS:11** ↔ **12** are similar, as the C-atoms connected to the migrating H-atom are both bound to an amide group. However, the internal angle surrounding the migrating H-atom (C–H–C) in **TS:11** ↔ **12**, which is an eight-membered ring, is 168.0° (*Fig. 5*), which is much wider than the corresponding angle in **TS:9c** ↔ **10c** (131.6°). As a result, reaction **F** has forward (77.1 kJ·mol^{-1}) and reverse (100.2 kJ·mol^{-1}) barriers that are 21–24 kJ·mol^{-1} lower than the values for reaction **E** (*Table 6*). In contrast, the changes in reaction enthalpy are approximately the same for reactions **E** (–25.7 kJ·mol^{-1}) and **F** (–23.2 kJ·mol^{-1}), consistent with the analogous chemical environments in the vicinity of the radical sites involving the migrating H-atom.

3.2.4. *[N ↔ N] Shifts of H-Atoms.* Isomerization of the (destabilized) amidyl-N-radical **13a** to the (stabilized) alkyl-substituted N-radical **14a** *via* a 1,4[N ↔ N]-H shift in reaction **G** (*Scheme 1*) is strongly exothermic (ΔE = –71.1 kJ·mol^{-1}). The forward rearrangement barrier ($E^{\ddagger}_{fwd}$ = 33.4 kJ·mol^{-1}) is small, while the reverse barrier

Table 6. *Barriers* ($E^{\ddagger}_{fwd}$ and $E^{\ddagger}_{rev}$) *and Reaction Enthalpies* (ΔE) *for [C ↔ C]-H and [N ↔ N]-H Shifts Computed at Various Levels of Theory* (0 K; in kJ·mol^{-1})[a])

	1,4[C ↔ C]-H Shift (**E**)			1,7[C ↔ C]-H Shift (**F**)			1,4[N ↔ N]-H Shift (**G**)		
	$E^{\ddagger}_{fwd}$	ΔE	$E^{\ddagger}_{rev}$	$E^{\ddagger}_{fwd}$	ΔE	$E^{\ddagger}_{rev}$	$E^{\ddagger}_{fwd}$	ΔE	$E^{\ddagger}_{rev}$
G3(MP2)-RAD	98.6	−25.7	124.3	77.1	−23.2	100.2	33.4	−71.1	104.5
CBS-QB3	97.8	−26.0	123.8	74.2	−22.4	96.7	30.5	−67.4	97.8
G3//B3-LYP	102.2	−24.6	126.8	77.0	−23.7	100.6	32.1	−70.7	102.7
UBMK/6-311++G(*3df,3pd*)[b])	98.3	−31.1	129.5	77.5	−28.7	106.2	31.0	−72.5	103.5
RBMK/6-311++G(*3df,3pd*)[b])	100.1	−31.7	131.8	78.5	−29.2	107.7	26.2	−79.3	105.5
UBMK/6-31+G(*d,p*)[b])	96.5	−29.9	126.4	72.6	−27.2	99.7	31.0	−72.2	103.3
UMPWB1K/6-311++G(*3df,3pd*)[b])	94.7	−29.4	124.1	80.3	−26.6	106.9	34.7	−72.9	107.6
RMPWB1K/6-311++G(*3df,3pd*)[b])	97.9	−29.8	127.7	82.8	−27.0	109.8	27.4	−83.6	110.9
UMPWB1K/6-31+G(*d,p*)[b])	96.1	−27.1	123.3	78.3	−24.4	102.7	36.5	−73.1	109.6
UB3-LYP/6-311++G(*3df,3pd*)[b])	95.2	−28.4	123.6	74.3	−26.0	100.3	25.5	−56.5	82.0
RB3-LYP/6-311++G(*3df,3pd*)[b])	96.7	−28.9	125.6	74.9	−26.4	101.4	23.3	−59.2	82.5
UB3-LYP/6-31+G(*d,p*)[b])	94.9	−25.8	120.7	72.3	−23.4	95.7	25.7	−55.8	81.5

[a]) See *Scheme 1*. [b]) UB3-LYP/6-31G(*d*) geometry and *ZPVE*.

($E^{\ddagger}_{rev} = 104.5$ kJ·mol^{-1}) is relatively large, partly due to the size and sign of ΔE (*Table 6*). The N−H−N angle is quite narrow at 130.8° (*Fig. 5*).

3.3. *Conformational Preorganization in Model Radicals Prior to H-Atom Migration.* In some cases, the peptide radicals would need to undergo conformational change in preparation for an H-atom migration. We have calculated the thermochemical parameters for such conformational isomerization for species involved in reactions **C** (*Fig. 6*), **E** (*Fig. 7*) and **G** (*Fig. 8*). Reaction **C** is the most complicated of these three processes (see *Scheme 1*), as there are pathway-bifurcation points associated with conformational changes both before (leading to **5ac**) and after (leading from **6ac**) the H-transfer transition structure **TS:5ac** ↔ **6ac**. On the N-radical side of reaction **C**, starting from the extended structure **5st**, the **5st** → **5sc** → **5ac** pathway is more favorable than the **5st** → **5at** → **5ac** pathway, because the barrier to the *trans* ↔ *cis* isomerization **5at** → **5ac** is quite high at *ca.* 65 kJ·mol^{-1}. On the C-radical side of reaction **C**, the **6ac** → **6at** → **6st** and **6ac** → **6sc** → **6st** pathways have similar energy requirements, although the former is somewhat less favorable, with a barrier to the *cis* → *trans* isomerization **6ac** → **6at** of *ca.* 38 kJ·mol^{-1}. For the sake of simplicity, only the energies for the lower-energy pathways are included in *Fig. 6*. We note that the results show only a minor dependence on the level of theory used (*Table 7*). Amide bonds resist rotation [30] and, in addition to the significant barrier to H-transfer, the *cis* ↔ *trans* isomerization barriers are the most significant features in *Fig. 6*. The relative energy of **TS:5sc** ↔ **5st** (47.7 kJ·mol^{-1}) is particularly notable, as it is only slightly lower than the relative energy of **TS:5ac** ↔ **6ac** (57.3 kJ·mol^{-1}), and this shows that preorganization may be comparable in energy demands to H-transfer. In this regard, we recall the observation [11] that in substrates with an amide bond connecting the sites participating in a 1,5[C ↔ N]-H shift, the H-migration rate was found to be faster than amide C−N bond rotation.

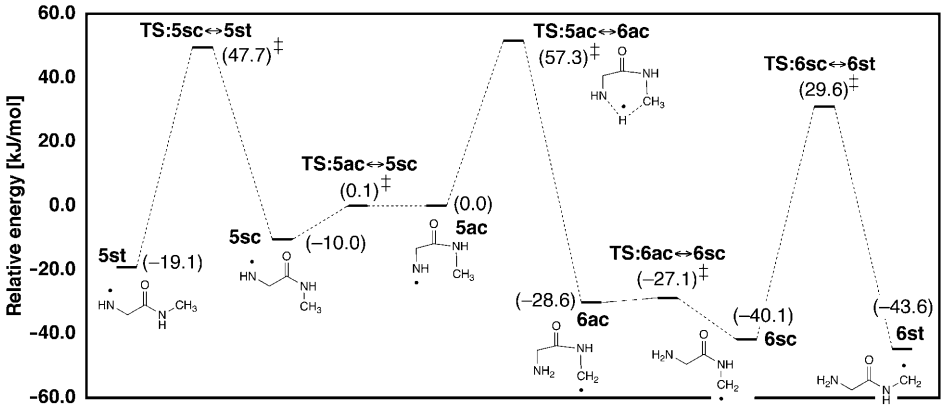

Fig. 6. *The* $^{\bullet}NH-CH_2-C(O)-NH-CH_3 \rightarrow NH_2-CH_2-C(O)-NH-CH_2^{\bullet}$ *1,5[C ↔ N]-H shift* (reaction **C**)*, including the barriers to* cis ↔ trans *and* syn-*periplanar* ↔ anti-*periplanar isomerization, at the G3(MP2)-RAD level of theory* (0 K)

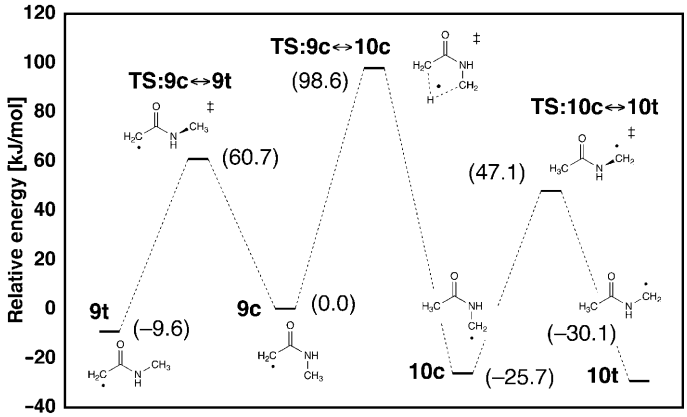

Fig. 7. *The* $^{\bullet}CH_2-C(O)-NH-CH_3 \rightarrow CH_3-C(O)-NH-CH_2^{\bullet}$ *1,4[C ↔ C]-H shift* (reaction **E**)*, including the barriers to* cis ↔ trans *isomerization, at the G3(MP2)-RAD level of theory* (0 K)

The barriers and enthalpies for *cis* ↔ *trans* isomerization about amide bonds in peptide radicals were also addressed for structures **9t**, **9c**, **10c**, and **10t** in reaction **E** (*Fig. 7*). As noted above, amide bonds resist rotation [30], and the considerable barriers for *cis* → *trans* isomerization for **9c** and **10c** in reaction **E** range from 60–73 kJ·mol^{-1}. In comparison, the G3(MP2)-RAD *cis* → *trans* barrier to amide bond rotation in *N*-methylacetamide (*Fig. 9*) is 70.7 kJ·mol^{-1}. An important observation for reaction **E** is that the rearrangement barrier for the 1,4[C ↔ C]-H shift is significantly larger than the barriers for *cis* → *trans* isomerization.

For the 1,4[N ↔ N]-H shift reaction **G**, the barrier to H-atom migration dominates the potential-energy profile (*Fig. 8*), as **TS:13a** ↔ **14a** lies *ca.* 105 kJ·mol^{-1} higher in energy than the global minimum **14a**. In contrast, the *anti*-periplanar → *syn*-periplanar isomerization barrier for **13a** → **13s** is very small (less than 1 kJ·mol^{-1}), while the **14a**

Table 7. *Thermochemical Parameters* [kJ·mol^{-1}] *for Preferred Rotational Isomerization Pathways for* **5**, **6**, **9**, **10**, **13**, *and* **14** (0 K)[a])

1,5[C ↔ N]-H Shift (**C**)	**5st** → **5sc**			**5sc** → **5ac**		
	$E^{\ddagger}_{fwd}$	ΔE	$E^{\ddagger}_{rev}$	$E^{\ddagger}_{fwd}$	ΔE	$E^{\ddagger}_{rev}$
G3(MP2)-RAD	66.8	9.1	57.7	10.0	10.0	0.1
CBS-QB3	69.0	9.3	59.7	10.3	10.3	0.0
UBMK/6-31+G(*d*,*p*)[b])	75.3	8.6	66.7	12.0	12.4	−0.3
UMPWB1K/6-31+G(*d*,*p*)[b])	76.9	9.1	67.8	14.4	14.7	−0.3
1,5[C ↔ N]-H Shift (**C**)	**6ac** → **6sc**			**6sc** → **6st**		
	$E^{\ddagger}_{fwd}$	ΔE	$E^{\ddagger}_{rev}$	$E^{\ddagger}_{fwd}$	ΔE	$E^{\ddagger}_{rev}$
G3(MP2)-RAD	1.5	−11.5	13.0	69.7	−3.5	73.1
CBS-QB3	1.4	−11.6	13.0	72.9	−2.9	75.7
UBMK/6-31+G(*d*,*p*)[b])	3.2	−11.9	15.1	78.5	−2.5	81.0
UMPWB1K/6-31+G(*d*,*p*)[b])	3.9	−12.9	16.9	78.8	−2.4	81.1
1,4[C ↔ C]-H Shift (**E**)	**9t** → **9c**			**10c** → **10t**		
	$E^{\ddagger}_{fwd}$	ΔE	$E^{\ddagger}_{rev}$	$E^{\ddagger}_{fwd}$	ΔE	$E^{\ddagger}_{rev}$
G3(MP2)-RAD	70.3	9.6	60.7	72.8	−4.4	77.2
CBS-QB3	70.1	9.3	60.7	74.1	−2.9	77.0
UBMK/6-31+G(*d*,*p*)[b])	78.5	8.9	69.6	82.1	−3.3	85.4
UMPWB1K/6-31+G(*d*,*p*)[b])	78.0	9.2	68.8	82.4	−3.5	85.8
1,4[N ↔ N]-H Shift (**G**)	**13s** → **13a**			**14a** → **14s**		
	$E^{\ddagger}_{fwd}$	ΔE	$E^{\ddagger}_{rev}$	$E^{\ddagger}_{fwd}$	ΔE	$E^{\ddagger}_{rev}$
G3(MP2)-RAD	12.8	12.1	0.7	19.0	7.7	11.3
CBS-QB3	12.1	10.4	1.7	18.7	7.4	11.4
UBMK/6-31+G(*d*,*p*)[b])	14.7	5.5	9.2	22.2	9.4	12.9
UMPWB1K/6-31+G(*d*,*p*)[b])	15.5	6.0	9.5	25.3	9.5	15.8

[a]) See *Scheme 1*. [b]) UB3-LYP/6-31G(*d*) geometry and *ZPVE*.

→ **14s** barrier is 19.0 kJ·mol^{-1} (*Fig. 8*). The *anti*-periplanar → *syn*-periplanar isomerization in the closed-shell analogue glycinamide (6.0 kJ·mol^{-1}, *Fig. 9*) lies between these values.

4. Conclusions. – The present study examines the thermochemistry of intramolecular H-atom transfer in small model systems related to truncated-peptide-backbone radicals, including an assessment of the performance of the various theoretical procedures employed. The following are the more important conclusions to emerge from this investigation:

1. The agreement between G3(MP2)-RAD and other high-level methods including G3//B3-LYP and CBS-QB3 in predicting enthalpies and barriers for the radical rearrangements is reasonable (*MAD*s <4 kJ·mol^{-1}), although there are deviations of up to 7 kJ·mol^{-1}. The computationally efficient hybrid-DFT methods UBMK/6-

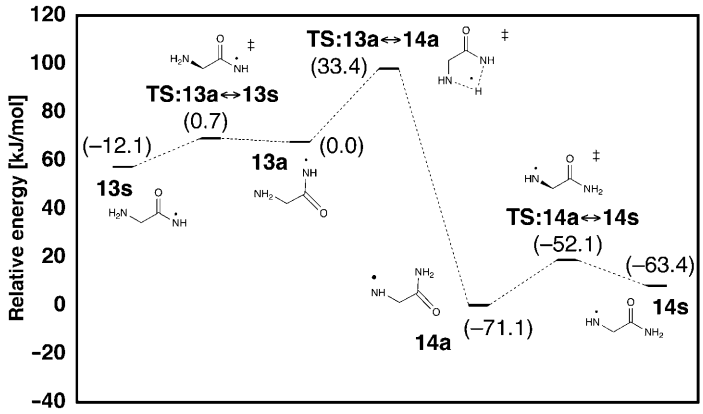

Fig. 8. *The* $^{\cdot}NH-CH_2-C(O)-NH_2 \rightarrow NH_2-CH_2-C(O)-NH^{\cdot}$ *1,4[N ↔ N]-H shift* (reaction **G**), *including the barriers to* syn-*periplanar* ↔ anti-*periplanar isomerization, at the G3(MP2)-RAD level of theory* (0 K)

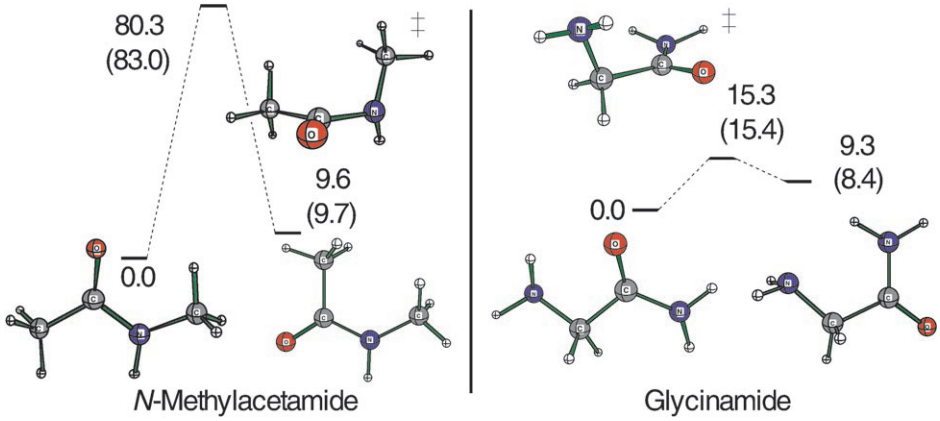

Fig. 9. *G3(MP2)-RAD and* (in parentheses) *CBS-QB3 thermochemical parameters* (0 K, in $kJ \cdot mol^{-1}$) *for isomerization of* N-*methylacetamide* (left) *and glycinamide* (right)

31+G(*d*,*p*) and UMPWB1K/6-31+G(*d*,*p*) also predict thermochemical parameters that are in good agreement with those from the high-level G3(MP2)-RAD procedure.

2. The exothermicities of rearrangements of N-radicals to C-radicals are quite large ($> 25\ kJ \cdot mol^{-1}$) and consequently, in some cases, *e.g.*, the 1,5[C ↔ N]-H and 1,6[C ↔ N]-H shifts, the rearrangements have relatively modest barriers ($< 60\ kJ \cdot mol^{-1}$).

3. C-Centered radicals are more stabilized by electron donation from an adjacent N-atom lone pair than delocalization into an adjacent carbonyl group, and consequently, the 1,4[C ↔ C]-H shift that converts $^{\cdot}CH_2-C(O)-NH-CH_3$ to $CH_3-C(O)-NH-CH_2^{\cdot}$ is exothermic (by $25.7\ kJ \cdot mol^{-1}$), as is the 1,7[C ↔ C]-H shift that converts $\cdot CH_2-C(O)-NH-CH_2-C(O)-NH-CH_3$ to $CH_3-C(O)-NH-CH_2-C(O)-NH-CH_2^{\cdot}$ (by $23.2\ kJ \cdot mol^{-1}$).

4. The enthalpy change ($-71.1\ kJ\cdot mol^{-1}$) and barrier ($33.4\ kJ\cdot mol^{-1}$) for the amidyl to amino 1,4[N ↔ N]-H shift ($NH_2-CH_2-C(O)-NH^{\bullet}$ to $^{\bullet}NH-CH_2-C(O)-NH_2$) are particularly favorable because of the relative destabilizing influence at the N-radical center of the CX=O group in the reactant on the one hand and the relative stabilizing influence of the CH_2Z group in the product on the other.

5. Calculations on prototypical systems show that H-transfer reactions prefer to proceed *via* linear or near-linear transition structures. This contributes to the observation that H-migration barriers generally decrease as the ring size in the TS increases. For example, a lowering of the barrier is found when moving from a rearrangement proceeding *via* a four-membered-ring TS (*e.g.*, the 1,3[C ↔ N]-H shift, $CH_3-C(O)-NH^{\bullet} \rightarrow {}^{\bullet}CH_2-C(O)-NH_2$) to a rearrangement proceeding *via* a six-membered-ring TS (*e.g.*, the 1,5[C ↔ N]-H shift, $^{\bullet}NH-CH_2-C(O)-NH-CH_3 \rightarrow NH_2-CH_2-C(O)-NH-CH_2^{\bullet}$).

We gratefully acknowledge the award of a University of Sydney Sesqui Postdoctoral Fellowship (to *D. M.*), funding from the *Australian Research Council* both for Discovery Grants and for the ARC Centre of Excellence in Free Radical Chemistry and Biotechnology (to *M. L. C.*, *M. J. D.*, *R. A. J. O.*, *C. J. E.*, and *L. R.*), and generous allocations of computing time (to *L. R.*) from the *Australian Partnership for Advanced Computing*, the *Australian National University Supercomputing Facility*, and the *Australian Centre for Advanced Computing and Communication*, and thank Professor *Jan Martin* for making the BMK functional available for our use.

REFERENCES

[1] C. J. Easton, *Chem. Rev.* **1997**, *97*, 53; N. L. Bauld, 'Radicals, Ion Radicals, and Triplets: the Spin-Bearing Intermediates of Organic Chemistry', Wiley-VCH, New York, 1997; C. J. Easton, in 'Radicals in Organic Synthesis. Vol. 2: Applications', Ed. P. Renaud and M. P. Sibi, Wiley-VCH, Weinheim, Germany, 2001; J. Stubbe, W. A. van der Donk, *Chem. Rev.* **1998**, *98*, 705; H. Eklund, M. Fontecave, *Struct. Fold. Des.* **1999**, *7*, R257; P. A. Frey, *Annu. Rev. Biochem.* **2001**, *70*, 121; D. T. Logan, J. Andersson, B.-M. Sjöberg, P. Nordlund, *Science (Washington, D.C.)* **1999**, *283*, 1499; C. J. Krieger, W. Roseboom, S. P. J. Albracht, A. M. Spormann, *J. Biol. Chem.* **2001**, *276*, 12924; S. T. Prigge, A. S. Kolhekar, B. A. Eipper, R. E. Mains, L. M. Amzel, *Science (Washington, D.C.)* **1997**, *278*, 1300.

[2] M. J. Davies, R. T. Dean, 'Radical-Mediated Protein Oxidation: from Chemistry to Medicine', Oxford University Press, Oxford, UK, 1997; K. B. Beckman, B. N. Ames, *Physiol. Rev.* **1998**, *78*, 547; S. Linton, M. J. Davies, R. T. Dean, *Exp. Gerontol.* **2001**, *36*, 1503.

[3] S. Fu, M. J. Davies, R. Stocker, R. T. Dean, *Biochem. J.* **1998**, *333*, 519.

[4] M. J. Davies, R. J. W. Truscott, *J. Photochem. Photobiol., B* **2001**, *63*, 114.

[5] A. Rauk, D. A. Armstrong, D. P. Fairlie, *J. Am. Chem. Soc.* **2000**, *122*, 9761.

[6] L. M. Sayre, M. G. Zagorski, W. K. Surewicz, G. A. Krafft, G. Perry, *Chem. Res. Toxicol.* **1997**, *10*, 518.

[7] C. L. Hawkins, D. I. Pattison, M. J. Davies, *Amino Acids* **2003**, *25*, 259; C. L. Hawkins, M. J. Davies, *Biochem. J.* **1998**, *332*, 617; C. L. Hawkins, M. J. Davies, *J. Chem. Soc., Perkin Trans. 2* **1998**, *12*, 2617.

[8] C. L. Hawkins, M. J. Davies, *J. Chem. Soc., Perkin Trans. 2* **1998**, *9*, 1937.

[9] F. Turecek, E. A. Syrstad, *J. Am. Chem. Soc.* **2003**, *125*, 3353; E. A. Syrstad, D. D. Stephens, F. Turecek, *J. Phys. Chem. A* **2003**, *107*, 115.

[10] T. Cohen, C. H. McMullen, K. Smith, *J. Am. Chem Soc.* **1968**, *90*, 6866; T. Cohen, K. W. Smith, M. D. Swerdloff, *J. Am. Chem. Soc.* **1971**, *93*, 4303.

[11] V. Snieckus, J. C. Cuevas, C. P. Sloan, H. T. Liu, D. P. Curran, *J. Am. Chem. Soc.* **1990**, *112*, 896.

[12] W. J. Hehre, L. Radom, J. A. Pople, P. v. R. Schleyer, 'Ab Initio Molecular Orbital Theory', John Wiley & Sons, Inc., New York, 1986.

[13] W. Koch, M. C. Holthausen, 'A Chemist's Guide to Density Functional Theory', Wiley-VCH, Weinheim, 2000.
[14] M. J. Frisch, G. W. Trucks, H. B. Schlegel, G. E. Scuseria, M. A. Robb, J. R. Cheeseman, J. A. Montgomery Jr., T. Vreven, K. N. Kudin, J. C. Burant, J. M. Millam, S. S. Iyengar, J. Tomasi, V. Barone, B. Mennucci, M. Cossi, G. Scalmani, N. Rega, G. A. Petersson, H. Nakatsuji, M. Hada, M. Ehara, K. Toyota, R. Fukuda, J. Hasegawa, M. Ishida, T. Nakajima, Y. Honda, O. Kitao, H. Nakai, M. Klene, X. Li, J. E. Knox, H. P. Hratchian, J. B. Cross, V. Bakken, C. Adamo, J. Jaramillo, R. Gomperts, R. E. Stratmann, O. Yazyev, A. J. Austin, R. Cammi, C. Pomelli, J. W. Ochterski, P. Y. Ayala, K. Morokuma, G. A. Voth, P. Salvador, J. J. Dannenberg, V. G. Zakrzewski, S. Dapprich, A. D. Daniels, M. C. Strain, O. Farkas, D. K. Malick, A. D. Rabuck, K. Raghavachari, J. B. Foresman, J. V. Ortiz, Q. Cui, A. G. Baboul, S. Clifford, J. Cioslowski, B. B. Stefanov, G. Liu, A. Liashenko, P. Piskorz, I. Komaromi, R. L. Martin, D. J. Fox, T. Keith, M. A. Al-Laham, C. Y. Peng, A. Nanayakkara, M. Challacombe, P. M. W. Gill, B. Johnson, W. Chen, M. W. Wong, C. Gonzalez, J. A. Pople, 'Gaussian 03', Wallingford CT, 2004.
[15] H.-J. Werner, P. J. Knowles, R. D. Amos, A. Bernhardsson, A. Berning, P. Celani, D. L. Cooper, M. J. O. Deegan, A. J. Dobbyn, F. Eckert, C. Hampel, G. Hetzer, T. Korona, R. Lindh, A. W. Lloyd, S. J. McNicholas, F. R. Manby, W. Meyer, M. E. Mura, A. Nicklass, P. Palmieri, R. Pitzer, G. Rauhut, M. Schütz, H. Stoll, A. J. Stone, R. Tarroni, T. Thorsteinsson, 'MOLPRO 2002.6', Cardiff University, UK, 2004.
[16] A. P. Scott, L. Radom, *J. Phys. Chem.* **1996**, *100*, 16502.
[17] A. D. Boese, J. M. L. Martin, *J. Chem. Phys.* **2004**, *121*, 3405.
[18] Y. Zhao, D. G. Truhlar, *J. Phys. Chem. A* **2004**, *108*, 6908.
[19] A. G. Baboul, L. A. Curtiss, P. C. Redfern, K. Raghavachari, *J. Chem. Phys.* **1999**, *110*, 7650.
[20] D. J. Henry, M. B. Sullivan, L. Radom, *J. Chem. Phys.* **2003**, *118*, 4849.
[21] D. J. Henry, C. J. Parkinson, L. Radom, *J. Phys. Chem. A* **2002**, *106*, 7927.
[22] J. A. Montgomery, M. J. Frisch, J. W. Ochterski, G. A. Petersson, *J. Chem. Phys.* **2000**, *112*, 6532; J. A. Montgomery, M. J. Frisch, J. W. Ochterski, G. A. Petersson, *J. Chem. Phys.* **1999**, *110*, 2822.
[23] J. M. L. Martin, S. Parthiban, in 'Quantum-Mechanical Prediction of Thermochemical Data', Ed. J. Cioslowski, Kluwer Academic, Dordrecht, 2001.
[24] G. P. F. Wood, D. J. Henry, L. Radom, *J. Phys. Chem. A* **2003**, *107*, 7985.
[25] L. A. Curtiss, K. Raghavachari, P. C. Redfern, V. Rassolov, J. A. Pople, *J. Chem. Phys.* **1998**, *109*, 7764.
[26] S. G. Lias, J. E. Bartmess, J. F. Liebman, J. L. Holmes, R. D. Levin, W. G. Mallard, *J. Phys. Chem. Ref. Data, Suppl. 1* **1988**, *17*, 1.
[27] G. P. F. Wood, D. Moran, R. Jacob, L. Radom, *J. Phys. Chem. A* **2005**, *109*, 6318.
[28] A. K. Croft, C. J. Easton, L. Radom, *J. Am. Chem. Soc.* **2003**, *125*, 4119.
[29] C. Isborn, D. A. Hrovat, W. T. Borden, J. M. Mayer, B. K. Carpenter, *J. Am. Chem. Soc.* **2005**, *127*, 5794.
[30] K. B. Wiberg, P. R. Rablen, D. J. Rush, T. A. Keith, *J. Am. Chem. Soc.* **1995**, *117*, 4261.

Received April 20, 2006